Journal of Molecular Structure 1278 (2023) 134929

Contents lists available at ScienceDirect

Journal of Molecular Structure

journal homepage: www.elsevier.com/locate/molstr

Effect of sulfur precursors on hydrothermal growth of MoS_2 nanostructures and its visible-light-driven photocatalytic activities

Zulfiqar Ali[a,*], Qadeer Hussain[b], Mirza Arfan Yawer[b,c,**], Mazhar Mehmood[a], Riaz Hussain[b], Attaullah Shah[e], Hira Kanwal[a,d], Affifa Yawer[f], Sajjad Ahmad[b], Sikandar Zahid[a]

[a] National Centre for Nanotechnology (NCN), Department of Metallurgy and Materials Engineering (DMME), Pakistan Institute of Engineering and Applied Sciences (PIEAS), Nilore, Islamabad 45650, Pakistan
[b] Department of Chemistry, University of Education, Punjab 32200, Pakistan
[c] Department of Chemistry, Division of Science and Technology, University of Education Lahore, Pakistan
[d] Department of Physics and Applied Mathematics (DPAM), Pakistan Institute of Engineering and Applied Sciences, Nilore, Islamabad 45650, Pakistan
[e] National Institute of Lasers and Optronics College, Pakistan Institute of Engineering and Applied Sciences, Nilore, Islamabad 45650, Pakistan
[f] RECETOX, Masaryk University, Faculty of Science Kamenice 753/5, building A29, Brno 62500, Czech Republic

ARTICLE INFO

Article history:
Received 17 October 2022
Revised 19 December 2022
Accepted 5 January 2023
Available online 6 January 2023

Keywords:
Hydrothermal synthesis
MoS_2 nanosheets
Dye degradation
Photocatalysis
Methyl orange (MO)

ABSTRACT

The molybdenum disulfide (MoS_2) nanostructures such as nanosheets, nanoflowers, nanoparticles, and nanoflakes are promising candidate materials for environmental pollution control. In this work, the effect of sulfur precursors i.e. thioacetamide, thiourea, and elemental sulfur on the morphology of hydrothermally grown MoS_2 material was studied followed by their visible-light-driven photocatalytic activities toward methyl orange (MO) dye degradation at ambient conditions. Interestingly under scanning electron microscope (SEM) images, the morphologies of synthesized materials were seen to consist of systematic nanosheets, aggregates, and agglomerates. Raman spectroscopy and XRD studies suggested that the grown materials were composed of primarily 1T-2H mixed phase of MoS_2 along with a minor oxide phase of molybdenum. Moreover, photocatalytic MO dye degradation activities exhibited by thioacetamide-grown MoS_2 nanostructures were found to be better than those of elemental sulfur and thiourea counterparts. The kinetic rates of degradation towards MO dye by materials synthesized with thioacetamide, elemental sulfur, and thiourea were found to be 0.00804 min^{-1}, 0.00614 min^{-1}, and 0.00531 min^{-1}, respectively. The relatively better photocatalytic activities exhibited by thioacetamide-grown MoS_2 material were attributed to its predominant nanosheet morphology and the presence of a greater amount of MoS_2 contents. This work will be helpful for a better understanding of morphological control hydrothermal synthesis of MoS_2-based materials and their subsequent organic dye degradation activities.

1. Introduction

MoS_2 is the typical example of 2D transition metal dichalcogenides (TMDs) material which has attracted the considerable attention of researchers across the globe due to its diversified applications including optoelectronics, nanoelectronics, sensing, photocatalytic dye degradation, energy storage, and conversion [1–7]. MoS_2 generally exists in three crystal structures i.e. 1T, 2H, and 3R phases in which T, H, and R represent the tetragonal, hexagonal and rhombohedral unit cells, respectively and the numeric 1, 2, and 3 in said crystal systems show the repetition of a particular layer in a unit cell [8–10]. Interestingly, the 1T-MoS_2 phase is metallic which has been widely exploited for electrocatalytic hydrogen evolution reaction (HER) [11,12]. On the other hand, 2H/3R phases have semiconducting properties and are considered promising photocatalytic materials [13,14]. MoS_2 due to its layered nature and high-temperature stability also finds use in solid-state lubricants [15,16]. In addition to the unique crystal structures of MoS_2, the morphology of MoS_2 nanostructured materials such as; nanosheets [17], nanoflowers [18], nanoflakes [19], nanotubes [20] and nanoparticles [21] are also of considerable interests owing to their interesting photocatalytic dye degradation properties [12]. For instance, Jaleel et al. [22] have synthesized MoS_2 nanoflowers by hydrothermal method and used these materials for malachite green (MG) dye degradation studies. Afsar et al. [23] have grown MoS_2 nanoflakes by solid-state method for

* Corresponding author.
** Corresponding author at: Department of Chemistry, University of Education, Punjab 32200, Pakistan.
E-mail addresses: alizulfiqar161@gmail.com (Z. Ali), mirza.yawer@ue.edu.pk (M.A. Yawer).

https://doi.org/10.1016/j.molstruc.2023.134929
0022-2860/

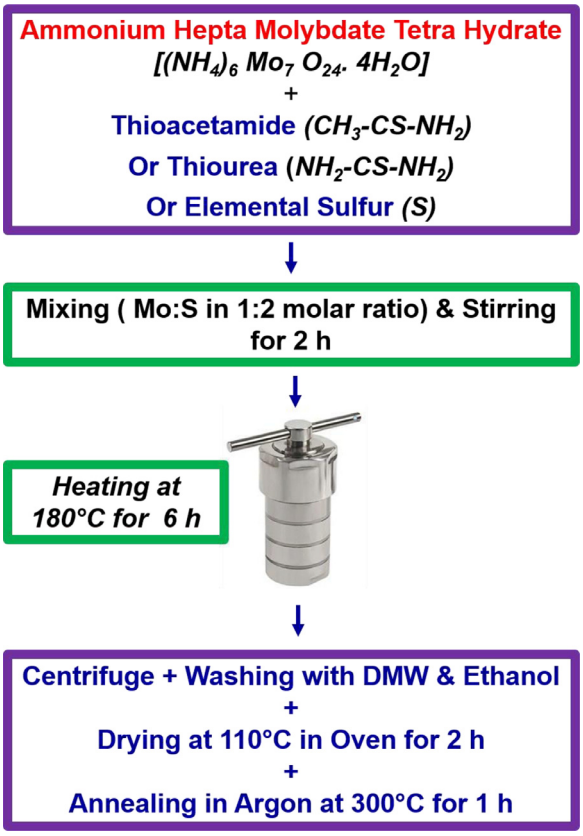

Fig. 1. Schematics for hydrothermal synthesis process for MoS_2 nanostructures.

photocatalytic methylene blue (MB) dye degradation. Chen et al. [24] have shown nanosheets composed of MoS_2 for photocatalytic rhodamine B dye degradation. Lee et al. [25] have studied the effect of pH over morphological control of MoS_2 nanostructures in which they demonstrated that the nanoparticles, aggregates, and nanoflowers of MoS_2 could be formed at acidic, neutral, and basic pH conditions, respectively. Choi et al. [26] have demonstrated the effect of temperature and pressure on the synthesis of MoS_2 and used it as catalytic material for methanation reaction. Khan et al. [27] have shown the effect of nickel doping on MoS_2 structure and evaluated the performance towards photocatalytic dye degradation methylene blue (MB), as well as rhodamine B (RhB), dyes under ultraviolet light (UV) irradiation. In another metal-doped MoS_2 work, Nazneen et al. [28] show the enhanced photocatalytic removal of organic dyes by silver-doped MoS_2 nanostructures. The 3D-MoS_2 nanoflowers have also been exploited for various organic dyes and antibiotic pollutant materials by Singh et al. [29]. Recently, ultrathin layered MoS_2 nanostructures have been synthesized by Sahoo et al. [30] for superior photodegradation properties towards methylene blue (MB), Malachite green (MG), and Rhodamine B (RhB) organic dye pollutants under visible light irradiation. Thus, it was found from the literature survey that the synthesis of MoS_2 nanostructures with various morphologies has considerable research interest in solving the environmental pollution problem caused by common organic dyes.

In our previous studies, we have demonstrated the synthesis of several carbon nanostructured materials for energy conversion reaction such as OER/HER and adsorption studies [31–42]. Herein motivated by fascinating and interesting morphologies of MoS_2 material, we report the study on the effect of sulfur precursor on morphology of MoS_2 material in typical hydrothermal growth conditions followed by their photocatalytic activities towards methyl orange (MO) dye degradation under visible light irradiation.

2. Materials and methods

2.1. Lab chemicals

Analytical reagent (AR) grade lab chemicals like ammonium hepta molybdate tetrahydrate $[(NH_4)_6Mo_7O_{24}{\cdot}4H_2O]$, thiourea $[(NH_2)CS(NH_2)]$, thioacetamide $[(CH_3)CS(NH_2)]$, elemental sulfur (S) granular powder; methyl orange (MO) dye, absolute ethanol, etc. were purchased from Merck company. De-mineralized water (DMW) was used for volume make-ups and washing of the products. All chemicals were used as-received without further purification.

2.2. Characterizations

Synthesized materials were characterized by the secondary electron microscope (SEM) model TESCAN at an operating voltage of 20 kV, Raman instrument model Raman Micro Ramboss spectrometer with a solid-state laser (λ = 532 nm), X-ray diffractometer Bruker D8 Discover with Cu Kα radiation, Carbon-Sulfur Analyzer instrument model (CSi-Eltra) Germany and bench top visible-spectrophotometer (wavelength range 380-900 nm).

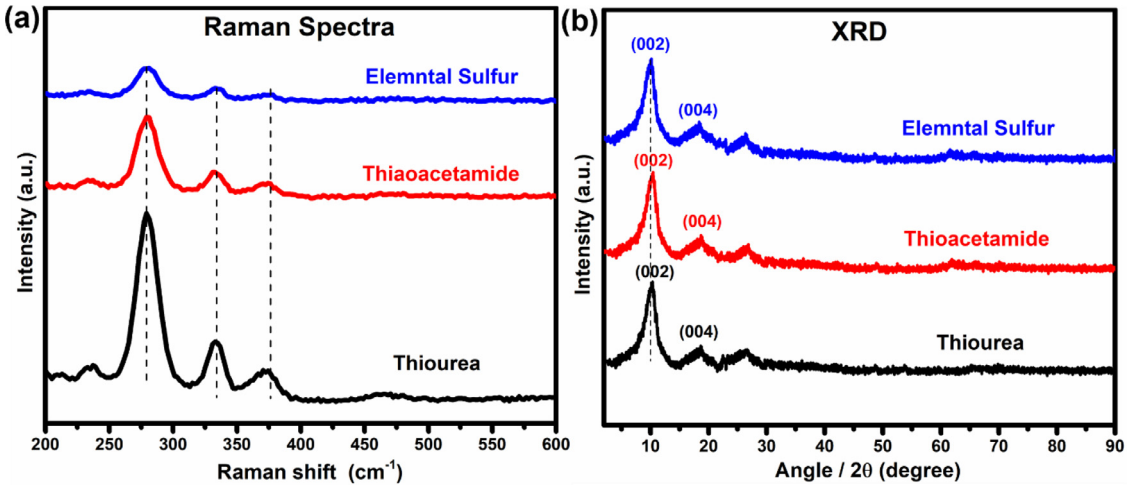

Fig. 2. Raman spectra (a) and XRD (b) of samples synthesized by hydrothermal method using different sulfur precursors.

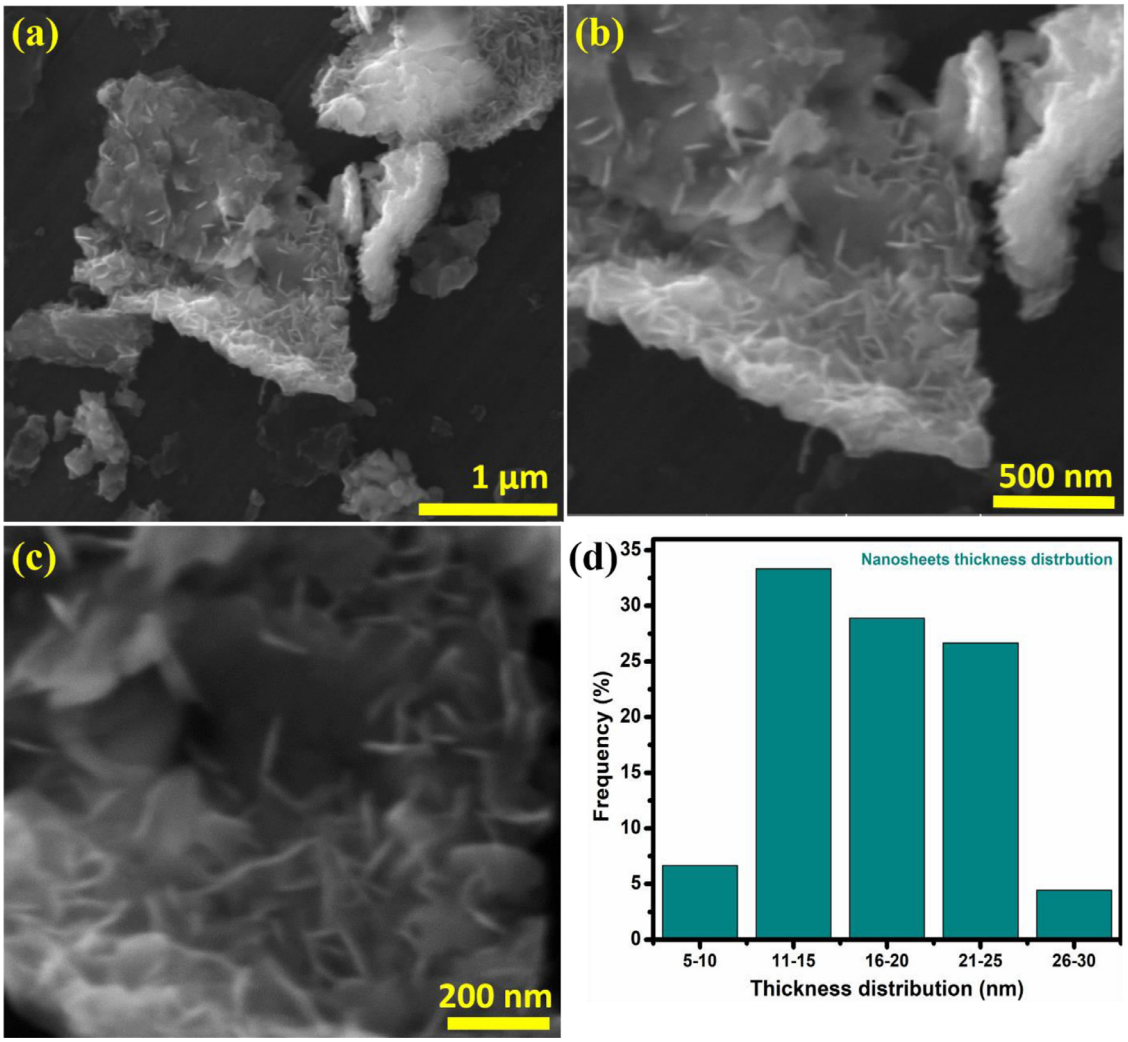

Fig. 3. (a), (b) low and (c) high magnification SEM images; (d) thickness distribution of nanosheets formed by hydrothermal method using thioacetamide.

2.3. Hydrothermal synthesis method for mos_2 nanostructures

The hydrothermal synthesis method for MoS_2 nanostructures was adopted from previous works [43–46] with some modifications. Typically 1.5 gs of ammonium hepta molybdate tetrahydrate and 1.5 gs of thioacetamide were taken in a 100 ml beaker followed by the addition of 50 ml DMW. The mixture was allowed to stir on the hotplate for 2 h to get a homogenized solution. Afterward, the solution was transferred into a Teflon-lined stainless steel autoclave and heated in an electric chamber furnace at a temperature of 180 °C for 6 h. The obtained powder material was washed several times with DMW and ethanol followed by drying in an oven at 110 °C for 2 h. The dried powder was then subjected to annealing in an argon atmosphere at 300 °C for 1 h. Similarly, the thiourea and elemental sulfur were used for the preparation of the other two samples instead of thioacetamide as a sulfur precursor. The schematic diagram for the complete synthesis process is shown in Fig. 1.

2.4. Photocatalytic activity measurement

Homemade photocatalytic reactor setup was used as shown schematically in supplementary information Fig. S1 by modifying the standard methods reported elsewhere [47–50]. The photocatalytic dye degradation studies were carried out by monitoring the decrease in the concentration of MO dye at regular intervals of time by measuring the concentrations of standard and samples at 435 nm wavelength. The experiments under exposure to light and without light were conducted in which the effect of photocatalyst dosage was also studied. The procedure for recycling of photocatalyst was as follows: first used 100 mg of photocatalysts contained in 100 ml of MO dye solution was centrifuged followed by decantation, washings with DMW, and drying in an oven at 110 °C for 2 h.

MO dye% removal was determined by using the following formula:

$$\%\mathbf{Removal} = [(\mathbf{Co} - \mathbf{Ct})/\mathbf{Co}] * \mathbf{100} \rightarrow \quad (1)$$

Where:

Ct = Concentration at a certain interval of time
Co = Initial concentration of MO Dye (5 ppm)

The rate constant "k" was determined by linear fitting the kinetic data into pseudo first order rate equation:

$$-\mathbf{lnCt}/\mathbf{Co} = \mathbf{kt} \rightarrow \quad (2)$$

Where;

k = Rate constant
Co = Initial concentration of MO dye
Ct = Concertation of MO at time t
t = Time interval

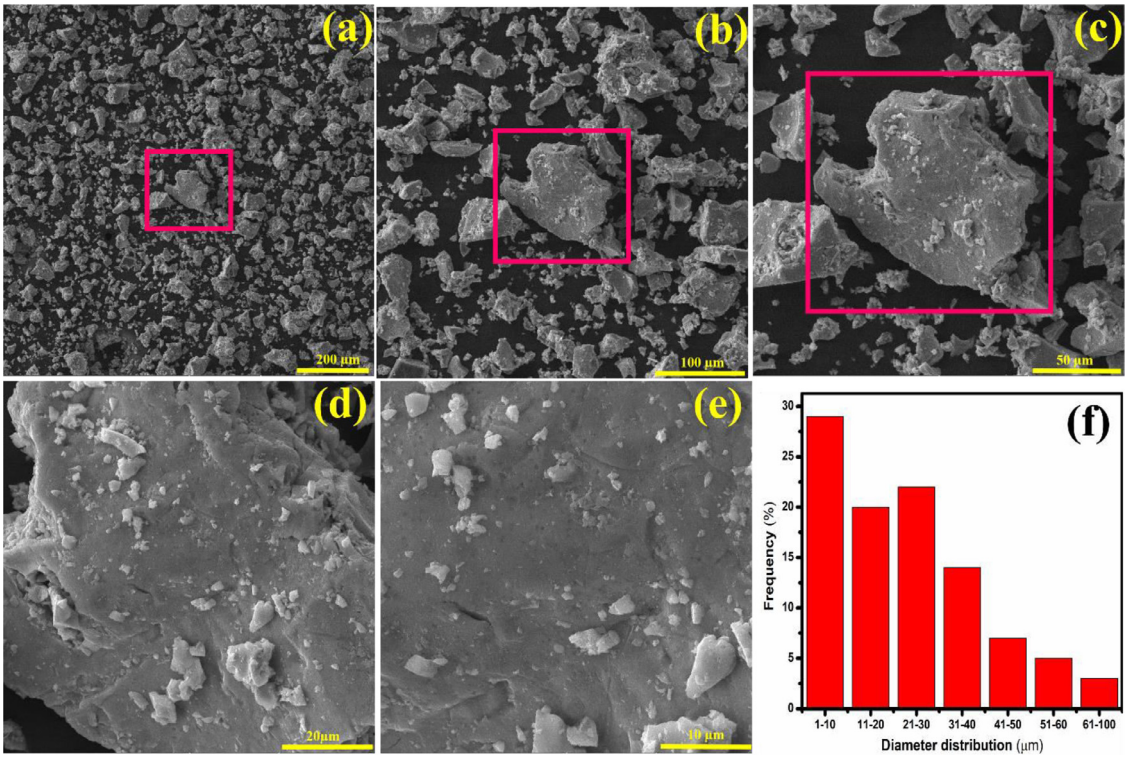

Fig. 4. SEM images (a-e) with increasing order of magnification and (f) diameter distribution of aggregates formed by hydrothermal method using thiourea.

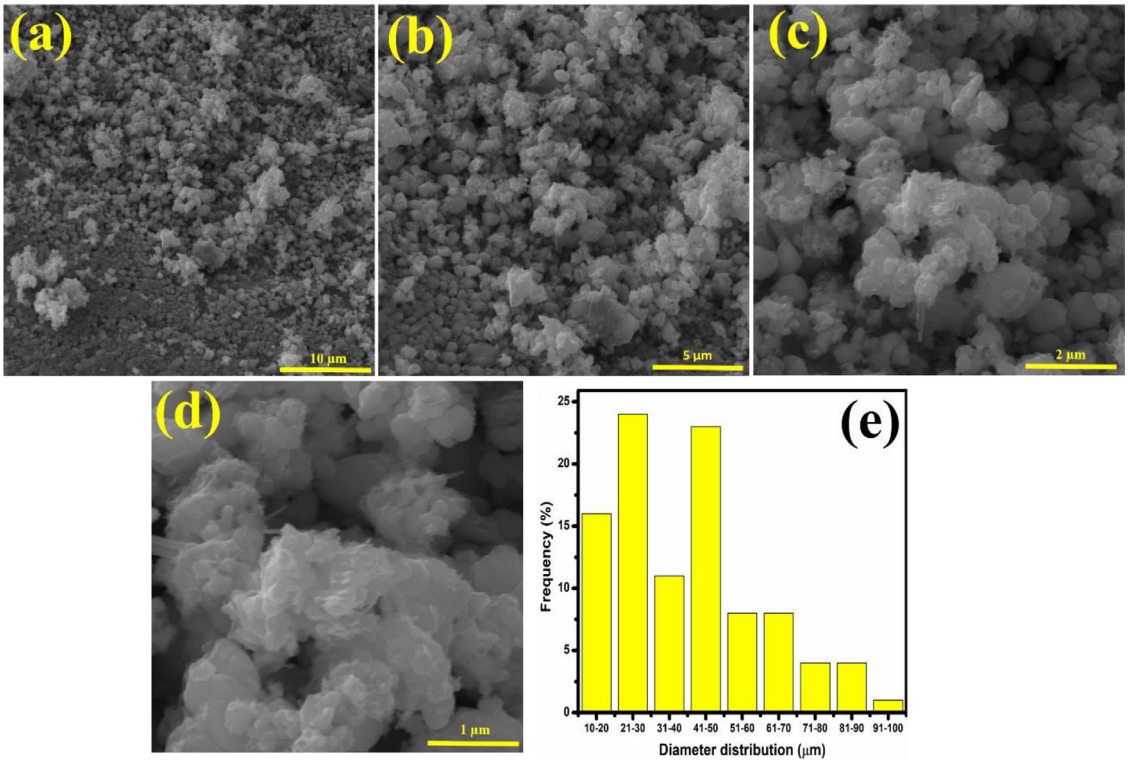

Fig. 5. SEM images (a-d) and (e) diameter distribution of agglomerates formed by hydrothermal method using elemental sulfur.

3. Result and discussion

The MoS_2 content in each sample was determined with the help of a carbon-sulfur (CS) analyzer which is the most reliable technique for sulfur determination in samples. Table 1 shows the results of sulfur contents along with corresponding MoS_2 amounts in all three synthesized samples. It can be seen that sample synthesized with thioacetamide has the highest amount of MoS_2 i.e. about 80% while the other two samples have relatively less amount of MoS_2 contents. The molybdenum precursor i.e. ammonium molybdate and all other experimental parameters were identical in three hydrothermal experiments, therefore, the role of sul-

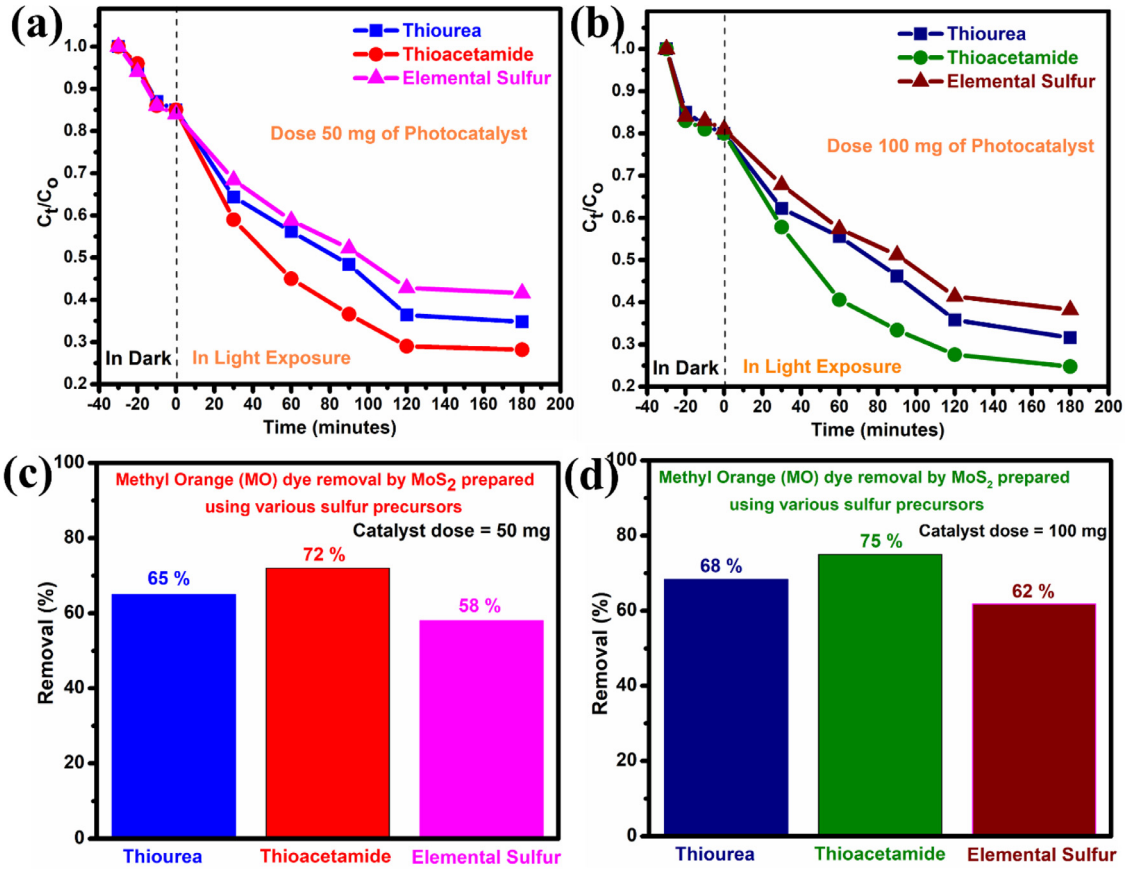

Fig. 6. Photocatalytic MO dye degradation curves (a,b) and corresponding% removals of dye (c, d) exhibited by three hydrothermally grown samples with catalyst dosages of 50 and 100 mg per 100 ml of 5 ppm MO solution.

Table 1
Sulfur and MoS_2 contents in synthesized samples with different sulfur precursors.

Sulfur (%)	MoS_2 (%)	Sulfur precursor
21.67	**54.18**	**Thiourea**
23.91	**59.78**	**Elemental Sulfur**
31.98	**79.94**	**Thioacetamide**

fur precursor seems to be the predominant factor in the yield of MoS_2.

Fig. 2(a) shows the Raman spectra of samples synthesized by the hydrothermal method at 180 °C temperatures for 6 h followed by annealing at 300 °C in an inert argon atmosphere using three different sulfur precursors. The main band positions for all three synthesized samples were around ~235 cm^{-1}, ~279 cm^{-1}, ~333 cm^{-1}, and ~373 cm^{-1} with slight shifts. These Raman bands are assigned to 1T-2H mixed phases by Saber et al. [51]. The minor shifts in peak positions may be attributed to different sulfur precursors used in typical hydrothermal synthesis methods for each sample. Fig. 2(b) shows the typical XRD patterns exhibited by the three synthesized samples under similar experimental conditions except for sulfur precursors. The sample synthesized with elemental sulfur, thioacetamide, and thiourea exhibit 2θ peaks at ~10.11° and ~18.34° which are indexed as (002) and (004) planes of MoS_2 material, interestingly these are typically known for mixed 2H@IT MoS_2 phase [52]. Fig. 2(b) also reveals the 2θ peaks around 26° for all three samples which are assigned to the oxide phase of molybdenum [53]. Thus, XRD and Raman's spectroscopy confirm the predominantly mixed phase of MoS_2 (1T-2H) in synthesized samples with a minor oxide phase.

Fig. 3(a) and (b) show the low magnification SEM images of the sample synthesized by hydrothermal method using thioacetamide as a sulfur precursor at 180 °C temperature for 6 h followed by annealing in an argon atmosphere at 300 °C. It can be seen that the overall morphology of the material is resembling assembled flowers nested in a vase. Fig. 3(c) shows the high magnification SEM image which clarifies that these assemblies are composed of nanosheets having a thickness of hierarchical order. The sheet thickness of the material was also determined which was found to be in the range of 5–30 nm with the predominant sheet thickness range lying in 11–25 nm. The sheet thickness distribution is shown in Fig. 2(d). Since Table 1 shows that the hydrothermally synthesized material with thioacetamide sulfur precursor contains about 80% of MoS_2 material, therefore these nanosheets are reasonably assigned to be composed of MoS_2 nanosheets. Similar morphology of nanosheets assigned to MoS_2 was observed in the work of Sun et al. [17].

Fig. 4(a-e) shows the SEM images of the sample synthesized by hydrothermal method using thiourea as a sulfur precursor under similar experimental conditions to those of thioacetamide-grown MoS_2 nanosheets. It can be seen in SEM images that the irregularly shaped aggregates of particles are predominant. Moreover, aggregate particles seem to tightly adhere to one another showing the dense cluster of particles that usually have strong interactions and bonds. The diameter distribution of the particles is shown in Fig. 4(f). It can be seen from the size distribution that the aggregate particle lies in the 1–100 μm range. The micron-sized aggregates are possibly composed of sulfides and oxides of molybdenum since MoS_2 contents in this sample are about 54 wt% (Table 1). The SEM observations along with MoS_2 contents determination in the sample synthesized by thiourea as sulfur precursor suggest that

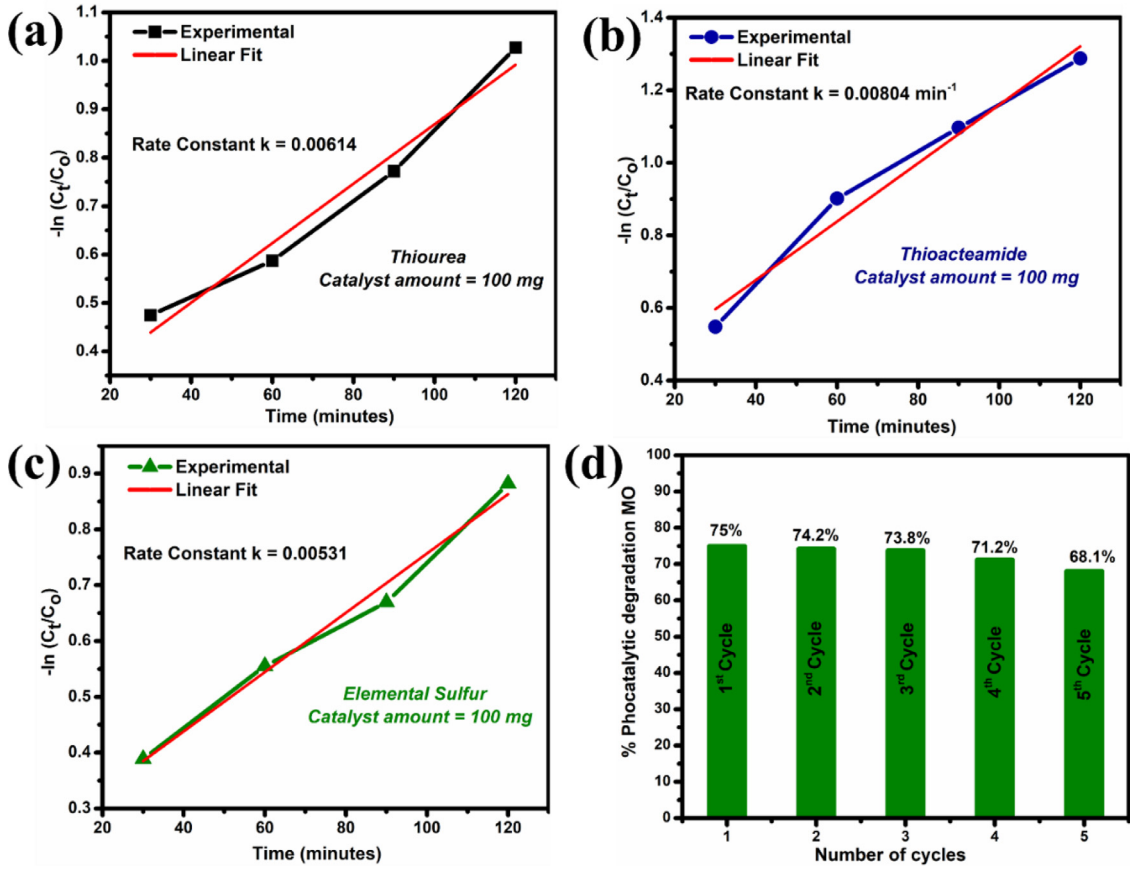

Fig. 7. Pseudo first order kinetic curves (a-c) exhibited by various synthesized materials and (d)% degradation of MO dye revealed up to 5th cycle by material synthesized using thioacetamide as a sulfur precursor under hydrothermal conditions.

the presented experimental conditions could yield a low yield of MoS_2 material with rough aggregate morphology.

Fig. 5(a-d) shows the SEM images of the sample synthesized by hydrothermal method using elemental sulfur precursor under identical hydrothermal conditions to those of thioacetamide and thiourea-grown MoS_2 materials. The increasing order of magnification from Fig. 5(a) to (d) suggests that this particular sample is full of loosely bound particles of micron-sized agglomerates i.e. less dense clusters of particles. The diameter distribution of the agglomerated particles is shown in Fig. 4(e). The diameter distribution of the agglomerated particles revealed that the micron-sized particles are in the range of 10-100 µm with predominant sizes from 10 to 40 µm. With the support of the amount of MoS_2 content results (Table 1), it may be assigned that the theses particles are predominately composed of MoS_2 agglomerates while balance material in the sample possibly is comprised of oxide impurity which sometimes grows in hydrothermally synthesized MoS_2 materials as shown in the previous work [17]. Since all three samples were synthesized in similar hydrothermal conditions yet the difference in MoS_2 contents and morphologies of the samples were observed which is attributed to the molecular structure difference of sulfur precursor. Thioacetamide (CH_3CSNH_2) due to methyl group presence in its structure possibly helped in reducing the environment and thus resulted in greater content of MoS_2 while thiourea (NH_2CSNH_2) and elemental sulfur (S) structures are devoid of methyl group and thus resulted in to the relatively lower amount of MoS_2.

Fig. 6(a-b) show the photocatalytic dye degradation curves with selected 50 mg and 100 mg dosage of photocatalysts under 200-watt visible light bulb irradiation as well as in dark at different time intervals. It can be seen that in dark the materials could remove about 20% MO dyes with respect to the initial 5 ppm concentration from the aqueous solution. The removal of MO dye in the absence of light may be attributed to the adsorption process. After 30 min time, all three synthesized materials degraded the MO dye very quickly and reaches saturation value in about 2 h. Fig. 6(c) shows the graphical representation of MO dye% removals with a catalyst dosage of 50 mg per 100 ml of 5 ppm MO dye and the% removals by samples synthesized using thiourea, thioacetamide, and elemental sulfur was found to be 65%, 72%, and 58%, respectively. Fig. 6(d) shows the% removals of MO dye with a catalyst dosage of 100 mg per 100 ml of 5 ppm solution. It was observed that by doubling the amount of photocatalyst the%removal of dye could increase up to 3–4%. It was also noticed that the MO degradation curves exhibited by thioacetamide-grown MoS_2 material showed relatively better photocatalytic performance than those of the other two counterpart samples. The better performance of said sample is presumably due to the presence of fine structure i.e. nanosheets which are often endowed with exposed edges, greater surface area, and facilitation of photocatalytic activities. Contrary to that other two synthesized materials possess predominant coarser structures i.e. agglomerate and aggregates, therefore these materials showed relatively low photocatalytic activities. Furthermore, it was found from the literature that the MoS_2 heterostructures are only capable of degrading MO dye over 90% [54]. But here, we found overall low catalytic performance by three synthesized samples i.e. (58–75%) which is possibly due to mixed-phase i.e. 2H/1T phase in which the 2H phase is the only semiconducting phase that contributes toward MO dye degradation. The predicted dye degradation mechanism as per previously published work [55–

58] is shown in supplementary information Fig.-S2. According to said published work when light falls on semiconductor material the electrons from the valence band (VB) jump to the conduction band (CB) thus leaving behind the negative and positive centers at CB and VB, respectively. Moreover, electrons at CB have the potential to reduce the free oxygen available in the system to superoxide (O2-) molecules while VB has the potential to convert water molecules into free radical (OH.) species. These superoxide and free radical species are collectively known as reactive oxidative species (ROS) which have enormous potential to decompose any of the organic dye into simpler compounds like CO_2 and H_2O [47]. We also believe that in our study the mechanism of MO dye degradation was of similar nature as discussed above.

Fig. 7(a-c) shows the experimental and linear fit of pseudo first order kinetics revealed for the sample synthesized by the hydrothermal method using three different sulfur precursors. The rate constants for samples having predominant nanosheets, aggregate, and agglomerate were found to be 8.04×10^{-2} min^{-1}, 6.14×10^{-2} min-1, and 5.31×10^{-2} min^{-1}, respectively which clearly indicates that the rate of degradation of MO dye exhibited by material composed of predominantly nanosheets is greater than those of aggregate and agglomerate materials. The fast kinetics on nanosheets is obvious because of its exposed edges and usually high surface area. Fig. 7(d) shows the% removals of dyes exhibited by a sample containing predominant MoS_2 nanosheets up to five cycles under similar conditions. It was observed that material after 5th recycling showed just about a 7% decrease in removal efficiency toward MO dye from aqueous solution. Moreover, its XRD spectra before and after the 5th recycle are shown in supplementary information Fig.-S3. There was no major change observed in the phase or composition of thioacetamide-grown photocatalytic material which is the hallmark of durable photocatalyst.

4. Conclusion

In the present work, the effect of three different sulfur precursors i.e. thiourea, thioacetamide, and elemental sulfur on the morphology of hydrothermally grown MoS_2 material was studied under similar experimental conditions. The sulfur precursor thioacetamide was found to be better for the growth nanosheet-like material while thiourea and elemental sulfur nucleated the materials composed of aggregate and agglomerates, respectively. The amount of MoS_2 contents in thioacetamide, thiourea, and elemental sulfur-grown material was found to be about 80%, 60%, and 54%, respectively. XRD and Raman spectroscopy studies revealed the presence of mixed-phase 1T-2H of MoS_2 in all three synthesized samples. The MO dye% removal exhibited by thioacetamide, thiourea, and elemental sulfur-grown materials were found to be 75%, 68%, and 62%, respectively under identical hydrothermal conditions with a rate constant 0.00804 min-1, 0.00614 min-1, and 0.00531 min-1. Moreover, in this study, the morphologically controlled hydrothermal synthesis of MoS_2-based nanosheet material was demonstrated using thioacetamide sulfur precursor.

Declaration of Competing Interest

The authors declare that they have no known competing financial interests or personal relationships that could have appeared to influence the work reported in this paper.

CRediT authorship contribution statement

Zulfiqar Ali: Conceptualization, Methodology, Investigation, Writing – review & editing, Supervision. **Qadeer Hussain:** Investigation, Writing – original draft, Formal analysis, Data curation. **Mirza Arfan Yawer:** Supervision, Resources, Project administration. **Mazhar Mehmood:** Writing – review & editing, Formal analysis. **Riaz Hussain:** Formal analysis, Project administration. **Attaullah Shah:** Formal analysis, Visualization. **Hira Kanwal:** Data curation, Formal analysis. **Affifa Yawer:** Visualization. **Sajjad Ahmad:** Data curation. **Sikandar Zahid:** Formal analysis.

Data availability

The authors are unable or have chosen not to specify which data has been used.

Supplementary materials

Supplementary material associated with this article can be found, in the online version, at doi:10.1016/j.molstruc.2023.134929.

References

[1] W. Choi, N. Choudhary, G.H. Han, J. Park, D. Akinwande, Y.H. Lee, Recent development of two-dimensional transition metal dichalcogenides and their applications, Mater. Today 20 (3) (2017) 116–130.
[2] Z. Li, X. Meng, Z. Zhang, Recent development on MoS_2-based photocatalysis: a review, J. Photochem. Photobiol. C 35 (2018) 39–55.
[3] U.C. Jaleel, K.R. Devi, D. Pinheiro, M.K. Mohan, Structural, morphological and optical properties of MoS_2-based materials for photocatalytic degradation of organic dye, Photochem 2 (3) (2022) 628–650.
[4] Q. Fu, J. Han, X. Wang, P. Xu, T. Yao, J. Zhong, W. Zhong, S. Liu, T. Gao, Z. Zhang, L. Xu, 2D transition metal dichalcogenides: design, modulation, and challenges in electrocatalysis, Adv. Mater. 33 (6) (2021) 1907818.
[5] L. Wang, D. Xu, L. Jiang, J. Gao, Z. Tang, Y. Xu, X. Chen, H. Zhang, Transition metal dichalcogenides for sensing and oncotherapy: status, challenges, and perspective, Adv. Funct. Mater. 31 (5) (2021) 2004408.
[6] D. Jiang, Z. Liu, Z. Xiao, Z. Qian, Y. Sun, Z. Zeng, R. Wang, Flexible electronics based on 2D transition metal dichalcogenides, J. Mater. Chem. A (2022).
[7] X. Zhang, G. Ma, J. Wang, Hydrothermal synthesis of two-dimensional MoS_2 and its applications, Tungsten 1 (1) (2019) 59–79.
[8] X. Zhang, H. Shi, L. Liu, C. Min, S. Liang, Z. Xu, Y. Xue, C. Hong, Z. Cai, Construction of MoS_2/Mxene heterostructure on stress-modulated kapok fiber for high-rate sodium-ion batteries", J. Colloid Interface Sci. 605 (2022) 472–482.
[9] I. Song, C. Park, H.C. Choi, Synthesis and properties of molybdenum disulphide: from bulk to atomic layers, RSC Adv. 5 (10) (2015) 7495–7514.
[10] X.L. Li, T.C. Li, S. Huang, J. Zhang, M.E. Pam, H.Y. Yang, Controllable synthesis of two-dimensional molybdenum disulfide (MoS_2) for energy-storage applications", ChemSusChem 13 (6) (2020) 1379–1391.
[11] S. Muralikrishna, K. Manjunath, D. Samrat, V. Reddy, T. Ramakrishnappa, D.H. Nagaraju, Hydrothermal synthesis of 2D MoS_2 nanosheets for electrocatalytic hydrogen evolution reaction", RSC Adv. 5 (109) (2015) 89389–89396.
[12] B. Han, Y.H. Hu, MoS_2 as a co-catalyst for photocatalytic hydrogen production from water, Energy Sci. Eng. 4 (5) (2016) 285–304.
[13] A. Rahman, J.R. Jennings, A.L. Tan, M.M. Khan, Molybdenum disulfide-based nanomaterials for visible-light-induced photocatalysis, ACS Omega 7 (26) (2022) 22089–22110.
[14] Y. Yuan, R.T. Guo, L.F. Hong, X.Y. Ji, Z.S. Li, Z.D. Lin, W.G. Pan, Recent advances and perspectives of MoS_2-based materials for photocatalytic dyes degradation: a review", Colloids Surf. A 611 (2021) 125836.
[15] P. Vattikuti, C. Byon, V. Reddy, B. Venkatesh, J. Shim, Synthesis and structural characterization of MoS_2 nanospheres and nanosheets using solvothermal method", J. Mater. Sci. 50 (14) (2015) 5024–5038.
[16] M.R. Vaziriserehk, A. Martini, D.A. Strubbe, M.Z. Baykara, Solid lubrication with MoS_2: a review", Lubricants 7 (7) (2019) 57.
[17] Y. Sun, J. Xu, Z. Zhu, Y. Wang, H. Xia, Z. You, C. Lee, C. Tu, Comparison of MoS_2 nanosheets and hierarchical nanospheres in the application of pulsed solid-state lasers", Opt. Mater. Express 5 (2015) 2924.
[18] J.S. Roy, G. Dugas, S. Morency, Y. Messaddeq, Rapid degradation of rhodamine B using enhanced photocatalytic activity of MoS_2 nanoflowers under concentrated sunlight irradiation", Physica E 120 (2020) 114114.
[19] J.-Y. Wu, M.-N. Lin, L.-D. Wang, T. Zhang, Photoluminescence of MoS_2 prepared by effective grinding-assisted sonication exfoliation", J. Nanomater. 2014 (2014) 1–7.
[20] B. Visic, R. Dominko, M.K. Gunde, N. Hauptman, S.D. Skapin, M. Remskar, Optical properties of exfoliated MoS_2 coaxial nanotubes-analogues of graphene", Nanoscale Res. Lett. 6 (2011) 593.
[21] M. Wojtalik, Z. Bojarska, Ł. Makowski, Experimental studies on the chemical wet synthesis for obtaining high-quality MoS_2 nanoparticles using impinging jet reactor", J. Solid State Chem. 285 (2020) 121254.
[22] U.C. Jaleel, K.R. Devi, P. Madhushree, Statistical and experimental studies of MoS_2/g-C_3N_4/TiO_2: a ternary Z-scheme hybrid composite", J. Mater. Sci. 56 (2021) 6922–6944.
[23] M.F. Afsar, M.A. Rafiq, F. Siddique, F. Saira, M.M. Chaudhary, M.M. Hasan, A.I.Y. Tok, Two-dimensional molybdenum disulphide nanoflakes synthesized by liquid-solid phase reaction method: regenerative photocatalytic perfor-

mance under UV-visible light irradiation by advance oxidation process, Mater. Res. Express 5 (5) (2018) 056206.
[24] W. Chen, M. Liu, S. Wei, X. Li, L. Mao, W. Shangguan, Solid-state synthesis of ultrathin MoS_2 as a co-catalyst on mesoporous g-C_3N_4 for excellent enhancement of visible light photoactivity", J. Alloy. Compd. 836 (2020) 155401.
[25] S.J. Lee, Y.S. Son, J.H. Choi, S.S. Kim, S.Y. Park, Morphology and catalytic performance of MoS_2 hydrothermally synthesized at various pH values", Catalysts 11 (10) (2021) 1229.
[26] J.M. Choi, S.H. Kim, S.J. Lee, S.S. Kim, Effects of pressure and temperature in hydrothermal preparation of MoS_2 catalyst for methanation reaction", Catal. Lett. 148 (7) (2018) 1803–1814.
[27] M.I. Khan, M.S. Hasan, K.A. Bhatti, H. Rizvi, A. Wahab, S.U. Rehman, M. Iqbal, Effect of Ni doping on the structural, optical and photocatalytic activity of MoS_2, prepared by Hydrothermal method, Mater. Res. Express 7 (1) (2020) 015061.
[28] A. Nazneen, M.I. Khan, M.A. Naeem, M. Atif, M. Iqbal, N. Yaqub, W.A. Farooq, Structural, morphological, optical, and photocatalytic properties of Ag-doped MoS_2 nanoparticles, J. Mol. Struct. 1220 (2020) 128735.
[29] J. Singh, S. Kumar, R.K. Soni, Synthesis of 3D-MoS_2 nanoflowers with tunable surface area for the application in photocatalysis and SERS based sensing", J. Alloy. Compd. 849 (2020) 156502.
[30] D. Sahoo, J. Shakya, N. Ali, W.J. Yoo, B. Kaviraj, Edge rich ultrathin layered MoS_2 nanostructures for superior visible light photocatalytic activity", Langmuir 38 (4) (2022) 1578–1588.
[31] Z. Ali, M. Mehmood, J. Ahmad, X. Li, A. Majeed, H. Tabassum, P.-.X. Hou, C. Liu, A platelet graphitic nanofiber-carbon nanotube hybrid for efficient oxygen evolution reaction, ChemCatChem 12 (1) (2020) 360–365.
[32] Z. Ali, M. Mehmood, J. Ahmad, A. Fatima, M. Ali, Fluorine doped CNTs for efficient OER activity outperforming iridium supported carbon electrocatalyst, J. Appl. Electrochem. 51 (2021) 1573–1581.
[33] Z. Ali, M. Mehmood, Z.A. Ghazi, Herring bone graphitic nanofibers grown on NiFe-silica nanocomposites by CVD method for HER activity in alkaline media, Mater. Lett. 305 (2021) 130838.
[34] Z. Ali, M. Mehmood, J. Ahmed, A. Majeed, K.H. Thebo, CVD grown defect rich-MWCNTs with anchored CoFe alloy nanoparticles for OER activity, Mater. Lett. 259 (2020) 126831.
[35] Z. Ali, M. Mehmood, J. Ahmad, M.T. Saleem, B. Ahmad, *In-situ* growth of novel CNTs-graphene hybrid structure on Ni-silica nanocomposites by CVD method for oxygen evolution reaction, Ceram. Int. 46 (11) (2020) 19158–19169.
[36] Z. Ali, M. Mehmood, J. Ahmad, M.T. Saleem, Catalytic growth of CNTs & carbon onions by chemical vapor deposition on nickel-silica nanocomposite and its electrochemical catalytic study towards OER, J. Porous Mater. 27 (6) (2020) 1571–1581.
[37] Z. Ali, M. Mehmood, J. Ahmad, S. Naz, Y. Khan, Heteroatoms (N, F, O)-doped CNTs on NiCo-silica nanocomposites for oxygen evolution reaction, Arab. J. Sci. Eng. 46 (1) (2021) 395–406.
[38] Z. Ali, M. Mehmood, J. Ahmad, M.N. Nizam, Synthesis of graphitic nanofibers and carbon nanotubes by CVD method on nickel chloride alcogel for excellent oxygen evolution reaction in alkaline media, Nanostruct. Nano Obj. 24 (2020) 100574.
[39] Z. Ali, M. Mehmood, J. Ahmad, A. Majeed, K.H. Thebo, MWCNTs and carbon onions grown by CVD method on nickel-cobalt alloy nanocomposites prepared via novel alcogel electrolysis technique and its oxygen evolution reaction application, Mater. Res. Express 6 (10) (2019) 105627.
[40] Z. Ali, M. Mehmood, J. Ahmad, M. Ali, T. Ghanni, S. Qamar, A. Fatima, Formation of carbon nanostructures on nickel acetate alcogel by CVD method and its OER electrocatalytic study in alkaline media, Appl. Phys. A 127 (9) (2021) 1–10.
[41] Z. Ali, M. Mehmood, M. Aslam, M.A. Haider, *In-situ* grown nickel-cobalt (NiCo) alloy nanoparticles decorated on petal-like nitrogen-doped carbon spheres for efficient OER activity, ChemistrySelect 7 (11) (2022) e202200196.
[42] Z. Ali, M.A. Khan, M. Mehmood, A. Shah, Catalytic growth of carbon nanowires on thin SS-410 sheet by CVD method and its adsorption behavior toward copper ions, Arab. J. Sci. Eng. (2022) 1–10.
[43] L. Ye, H. Xu, D. Zhang, S. Chen, Synthesis of bilayer MoS_2 nanosheets by a facile hydrothermal method and their methyl orange adsorption capacity", Mater. Res. Bull. 55 (2014) 221–228.
[44] M. Mulu, D. RamaDevi, N. Belachew, K. Basavaiah, Hydrothermal green synthesis of MoS 2 nanosheets for pollution abatement and antifungal applications, RSC Adv. 11 (40) (2021) 24536–24542.
[45] X. Zhang, H. Tang, M. Xue, C. Li, Facile synthesis and characterization of ultrathin MoS_2 nanosheets", Mater. Lett. 130 (2014) 83–86.
[46] K. Dharamalingam, B.A. Kumar, G. Ramalingam, S.S. Florence, K. Raju, P.S. Kumar, S. Govindaraju, E. Thangavel, The role of sodium dodecyl sulfate mediated hydrothermal synthesis of MoS_2 nanosheets for photocatalytic dye degradation and dye-sensitized solar cell application", Chemosphere 294 (2022) 133725.
[47] K. Kadiya, S.B. Vuggili, U.K. Gaur, M. Sharma, Comparative photocatalytic dye and drug degradation study using efficient visible light–induced silver phosphate nanoparticles", Environ. Sci. Pollut. Res. 28 (34) (2021) 46390–46403.
[48] A. Alshehri, M.A. Malik, Z. Khan, S.A. Al-Thabaiti, N. Hasan, Biofabrication of Fe nanoparticles in aqueous extract of Hibiscus sabdariffa with enhanced photocatalytic activities, RSC Adv. 7 (40) (2017) 25149–25159.
[49] F. Mirhoseini, A. Salabat, Ionic liquid based microemulsion method for the fabrication of poly(methyl methacrylate)–TiO_2 nanocomposite as a highly efficient visible light photocatalyst", RSC Adv. 5 (17) (2015) 12536–12545.
[50] N.N. Mohammad Jafri, J. Jaafar, N.H. Alias, S. Samitsu, F. Aziz, W.N. Wan Salleh, M.Z. Mohd Yusop, M.H.D. Othman, M.A. Rahman, A.F. Ismail, T. Matsuura, Synthesis and characterization of titanium dioxide hollow nanofiber for photocatalytic degradation of methylene blue dye, Membranes 11 (8) (2021) 581.
[51] M.R. Saber, G. Khabiri, A.A. Maarouf, M. Ulbricht, A.S. Khalil, A comparative study on the photocatalytic degradation of organic dyes using hybridized 1T/2H, 1T/3R and 2H MoS_2 nano-sheets", RSC Adv. 8 (46) (2018) 26364–26370.
[52] L. Tian, R. Wu, H. Liu, Synthesis of Au-nanoparticle-loaded 1T@ 2H-MoS_2 nanosheets with high photocatalytic performance", J. Mater. Sci. 54 (13) (2019) 9656–9665.
[53] J. Xie, K. Zhu, J. Min, J.Luo L.Yang, J. Liu, M. Lei, R. Zhang, L. Ren, Z. Wang, *In-situ* grown ultrathin MoS_2 nanosheets on MoO_2 hollow nanospheres to synthesize hierarchical nanostructures and its application in lithium-ion batteries", Ionics 25 (4) (2019) 1487–1494 *(Kiel)*.
[54] X. Liu, F. Meng, B. Yu, H. Wu, Self-assembly synthesis of flower-like CeO_2/MoS_2 heterojunction with enhancement of visible light photocatalytic activity for methyl orange", J. Mater. Sci. Mater. Electron. 31 (9) (2020) 6690–6697.
[55] X. Zhang, M. Xia, F. Wang, W. Lei, Cu_2O/MoS_2 composites: a novel photocatalyst for photocatalytic degradation of organic dyes under visible light, Ionics 26 (12) (2020) 6359–6369 *(Kiel)*.
[56] N. Tahir, M. Zahid, I.A. Bhatti, Y. Jamil, Fabrication of visible light active Mn–doped Bi_2WO_6-GO/MoS_2 heterostructure for enhanced photocatalytic degradation of methylene blue", Environ. Sci. Pollut. Res. 29 (5) (2022) 6552–6567.
[57] Y. Ye, Y. Feng, H. Bruning, D. Yntema, H.H.M. Rijnaarts, Photocatalytic degradation of metoprolol by TiO_2 nanotube arrays and UV-LED: effects of catalyst properties, operational parameters, commonly present water constituents, and photo-induced reactive species, Appl. Catal. B 220 (2018) 171–181.
[58] M. Ikram, A. Raza, M. Imran, A. Ul-Hamid, A. Shahbaz, S. Ali, Hydrothermal synthesis of silver decorated reduced graphene oxide (rGO) nanoflakes with effective photocatalytic activity for wastewater treatment, Nanoscale Res. Lett. 15 (1) (2020) 1–11.